Case study: Identification of brake squeal source mechanism through experimental and computational approaches

Ömer Anıl Tozkoparan[a)], Osman Taha Sen[b)] and Rajendra Singh[c)]

(Received: 2 August 2018; Revised: 14 August 2019; Accepted: 27 November 2019)

In this case study, mechanism leading to squeal noise in an automotive disc brake system is investigated with focus on systematic laboratory experiments and associated computational models. First, experimental modal analyses are conducted on the brake corner assembly components, and the natural frequencies and corresponding mode shapes are obtained. Second, finite element models of same components are developed, updated and validated by comparing predicted modal characteristics with those measured. Third, a controlled laboratory experiment is designed, constructed and operated in a semi-anechoic room. Experiments are conducted at many operational disc speeds and brake line pressures, and acceleration on the caliper and sound pressure are measured. Squeal events at distinct frequencies are successfully identified in the experiments. Fourth, a comprehensive computational model of the brake corner assembly is constructed using validated component models, and squeal investigation is then conducted through complex eigenvalue analyses while mimicking the operational conditions of experiments. The system model yields unstable frequencies at several operational conditions. It is observed that experimentally detected squeal frequencies match well with predicted unstable frequencies. Finally, operational deflection shape measurements on the caliper are also carried out during squeal events, and the predictions are found to be similar to those measured. In conclusion, the squeal generation mechanism of the brake system is understood from the perspective of friction-induced modal coupling, and an experimentally validated computational model of the brake system is successfully developed that may be used to find solutions to mitigate squeal.

Primary subject classification: 11.8.1; Secondary subject classification: 75.6

1 INTRODUCTION

The brake squeal noise problem (beyond 1 kHz) is a major source of customer dissatisfaction for automobile manufacturers[1–3], and a significant number of brake system related warranty issues are claimed to be linked to squeal[4]. Among many friction-induced vibration and noise problems, the brake squeal has also attracted most attention from academic researchers, as evident from three comprehensive literature reviews[1–3]. Several physical mechanisms leading to squeal noise have been proposed; these include negative damping concept, dynamic instability due to mode coupling, stick-slip, sprag-slip and hammering[1]. However, the problem still remains elusive, and no general noise control solution has been proposed yet due to its nonlinear and/or random characteristics.

Squeal phenomenon has been extensively studied by experimental[5–7], computational[8–10] and analytical[11,12] approaches. For the experimental investigations of squeal, few laboratory setups have been built, such as pin-on-disc, beam-on-disc, and mass on sliding belt, as well as test rigs with simple brake components[13]. As an example, Giannini et al.[6] built an experiment where an elastic beam is used as the caliper; they claim that the squeal frequencies are usually close to the natural frequencies of the coupled system, and the stick-slip vibrations are not essential to initiate squeal. Furthermore, the effect of relative velocity change (between the brake disc and brake pad) on a shift in the squeal frequency is found to be insignificant[6]. In

a) TU Dortmund, Faculty of Mechanical Engineering, Department of Materials Test Engineering, Dortmund, Germany; email: anil.tozkoparan@tu-dortmund.de.
b) Istanbul Technical University, Department of Mechanical Engineering, Istanbul, Turkey; email: senos@itu.edu.tr.
c) The Ohio State University, Department of Mechanical and Aerospace Engineering, Columbus, OH, USA; email: singh.3@osu.edu.

another experimental study, Butlin and Woodhouse[5] performed a large number of squeal tests on a pin-on-disc setup and explored an initiation of squeal events. They claim that the normal pre-load, disc speed and additional masses attached on the pin assembly lead to shifts in the squeal frequencies. In terms of the computational approaches, finite element models based on the complex eigenvalue analysis (for a linearized system) and transient time domain analysis (for a nonlinear system) are employed to evaluate the squeal propensity of particular brake systems[14]. The complex eigenvalue analysis method is the preferred technique in the automotive industry due to its ease and computational efficiency when compared to the time domain analyses[9,15]. Nevertheless, this approach may lead to wrong calculations and may identify too many unstable modes[16]. Furthermore, the finite element models of brake system assemblies[15,17] must be properly updated to refine the representative structural or vibro-acoustic models.

The chief goal of this article is to describe the experimental and computational steps taken to identify the squeal source mechanism in a particular automotive disc brake sub-system without involving the complicating effect of vehicle transfer paths. The system is assumed to be linear, and the friction excitation is included in the model in a simplified manner. Accordingly, the main

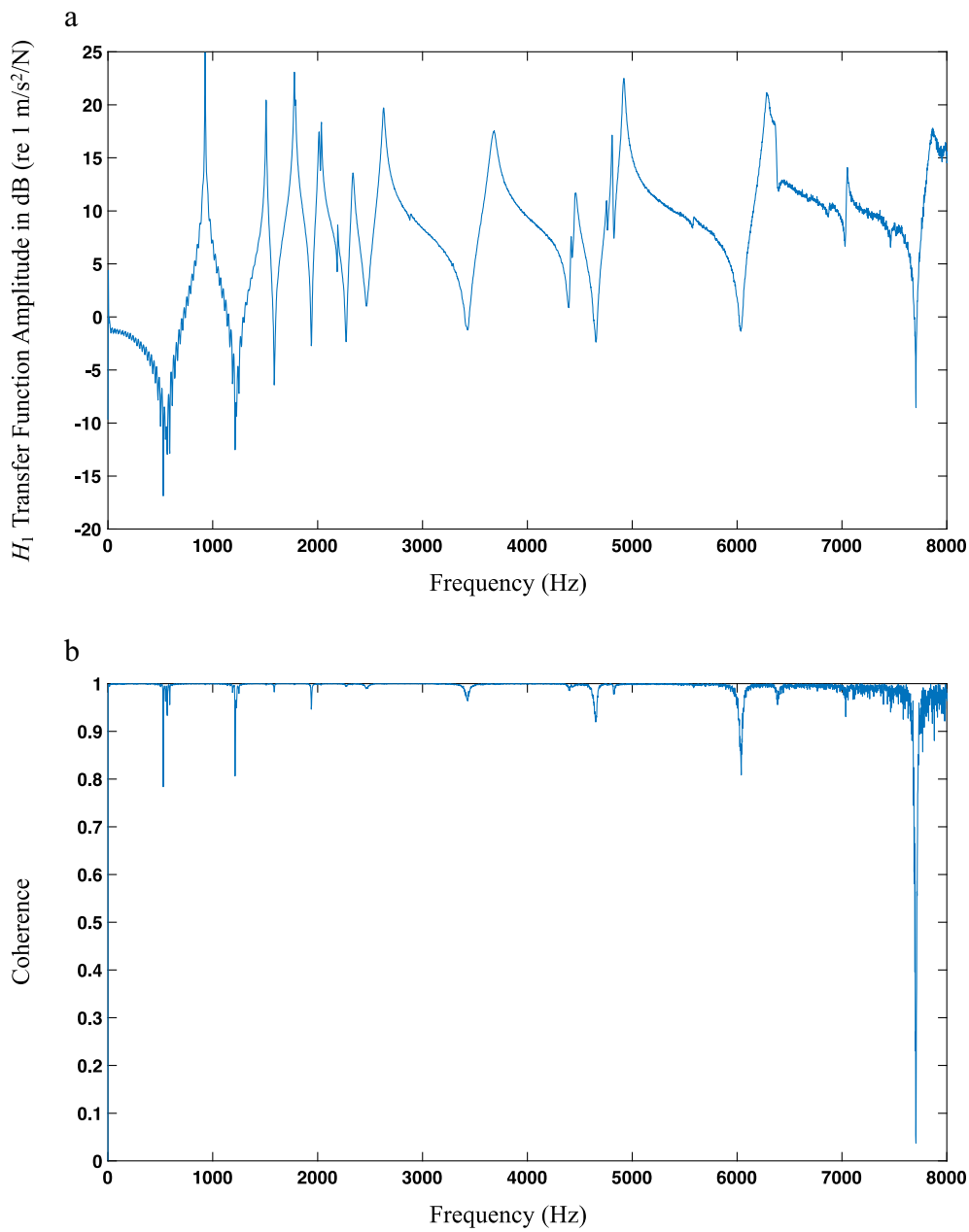

Fig. 1—Modal experiment result for the brake disc. (a) Transfer function magnitude at the driving point; (b) Coherence.

objectives (or major tasks) are as follows: 1) determine the modal characteristics (natural frequencies and mode shapes) of brake system components (under free-free conditions) through modal testing; 2) develop, update and validate finite element models of the corresponding brake components; 3) design and build a simplified laboratory experiment, perform squeal tests at key operational conditions, and identify dominant squeal events; 4) develop a finite element model of the system (brake corner assembly) using validated component models and investigate the squeal events through the complex eigenvalue analysis; and 5) compare experimental and computational results to determine the nature of model coupling and thus the mechanism of squeal noise. Well-recognized methods are utilized though intense efforts are still needed to correlate theory and experiment at each step.

2 MODAL ANALYSIS OF BRAKE COMPONENTS

2.1 Experimental Modal Analysis

In order to understand the modal characteristics (natural frequencies and mode shapes) of brake system components, experimental modal analysis (EMA) is first utilized. Modal tests are conducted under free-free boundary conditions that are approximated by suspending the brake system components with fishing line. The excitation force is applied with an impact hammer, and the accelerance type

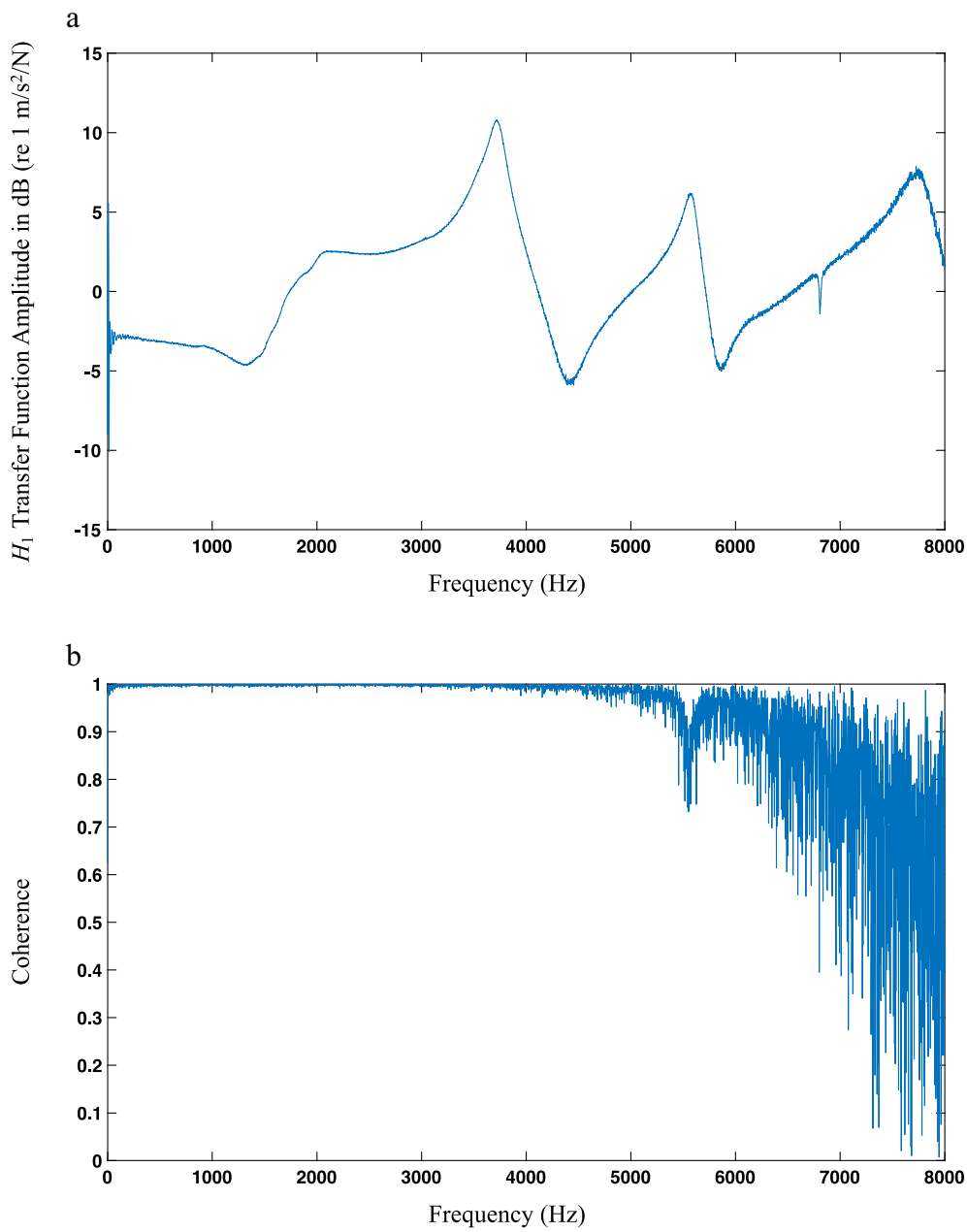

Fig. 2—Modal experiment result for the brake pad. (a) Transfer function magnitude at the driving point; (b) Coherence.

frequency response functions are measured at four different locations with uniaxial accelerometers for each component of the brake system. Additionally, the roving hammer technique is used to enhance the spatial resolution of the extracted mode shapes. The modal testing of the brake disc is performed first with 25 excitation points, where 16 of them are on the friction disc and the rest are on the hat section. Due to the geometries of the brake disc (and the pad), only in plane modes are expected. Therefore, excitation and measurement directions are chosen accordingly. The brake pads are tested similarly, though only 9 excitation points are chosen. Given the complex geometries of the caliper and the carrier, the measurement and excitation points have to be normal to the surface for a precise representation of the mode shape. Hence, the caliper and the carrier are tested with 10 and 13 excitation points, respectively, where each point is excited at three orthogonal directions (x, y, z).

Illustrative measured driving point transfer functions and coherences for brake disc, brake pad, caliper and carrier are shown in Figs. 1 to 4, respectively. Observe that the measured accelerances for the brake disc, brake pad and carrier are reliable over the entire frequency range (up to 8 kHz) as evident from the corresponding coherence spectra. However, the frequency response function of the caliper is depicted only up to 4 kHz due to poor coherence at the higher frequencies. This is probably due to the insufficient excitation energy and/or complexity of the

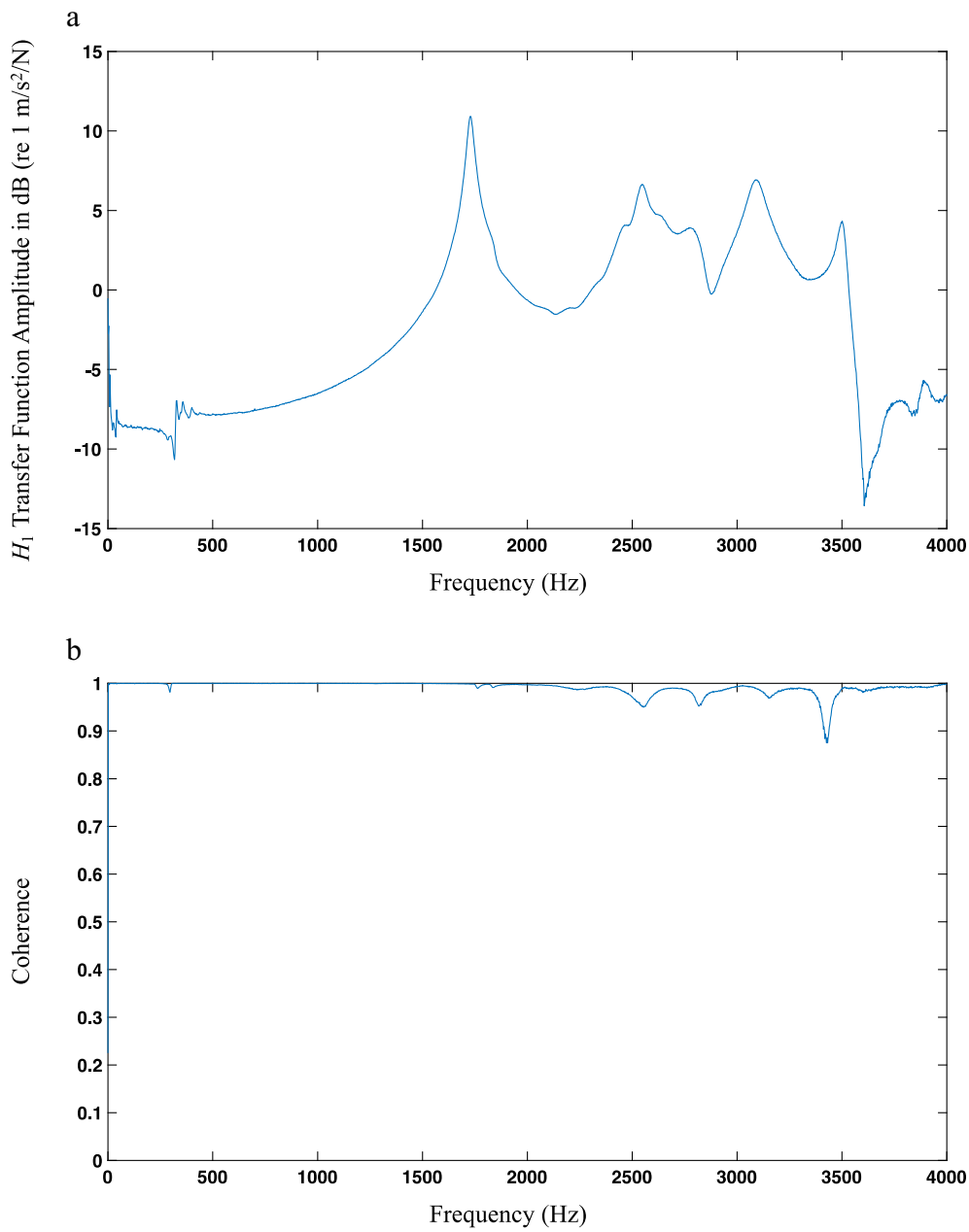

Fig. 3—Modal experiment result for the caliper. (a) Transfer function magnitude at the driving point; (b) Coherence.

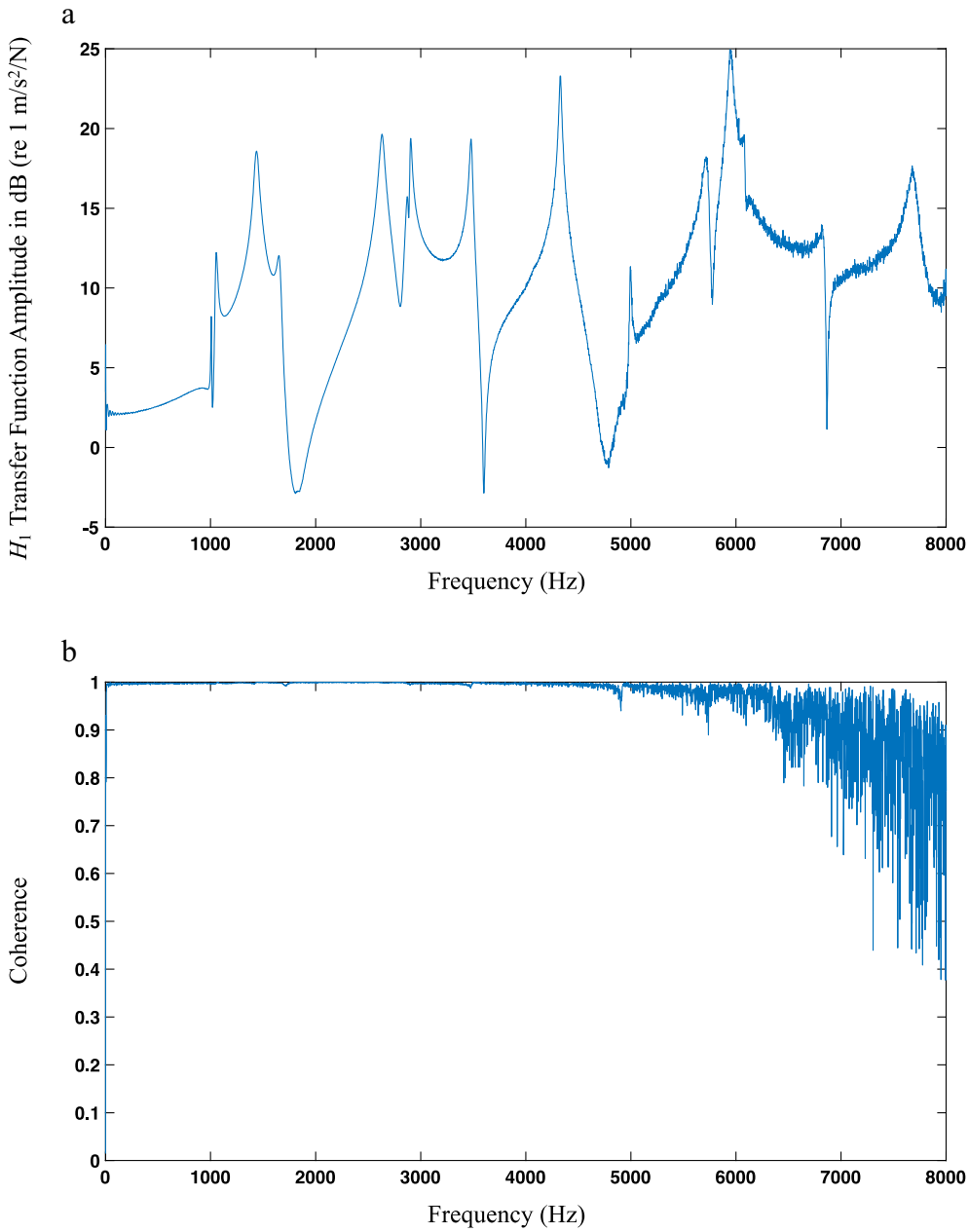

Fig. 4—Modal experiment result for the carrier. (a) Transfer function magnitude at the driving point; (b) Coherence.

caliper geometry. Furthermore, it is seen in Fig. 2(b) and 4(b) that the brake pad and carrier coherence spectra are distorted beyond 6 kHz; this is most probably due to the nonlinear behavior of the brake pad friction material, geometry of the carrier and inadequate excitation beyond 6 kHz.

Mode shapes obtained from the experimental modal analysis are determined by quadrature picking technique[18], since all the components tested are expected to be lightly damped. This is also observed from the measured frequency response functions where coincident spectra are insignificant compared to quadrature spectra. Hence, the imaginary parts are assumed to be strongly related with the modal amplitudes.

2.2 Computational Modal Analysis

Finite element models (FEMs) of the brake components are constructed with a commercial software (ABAQUS). Some features of these models are summarized in Table 1. First, the mesh convergence of each component is analyzed to obtain an optimum mesh size for accurate results. Second, the FEM solutions are obtained under free-free boundary conditions and complex eigenvalues, and natural

Table 1—Summary of finite element models of brake system components.

Brake component		Number of elements	Element type in ABAQUS*
Brake disc		4628	Eight node brick element (C3D8)
Brake pad	Backing plate	698	Eight node brick element (C3D8)
	Friction material	1344	Eight node brick element (C3D8)
Caliper		21768	Ten node tetrahedral element (C3D10)
Carrier		12300	Ten node tetrahedral element (C3D10)

*See Ref. 19 for an explanation the element types.

frequencies and corresponding mode shapes of each brake component are calculated. Predicted results are compared with measured data, and finally the finite element models are updated for improved correlation. The model updating procedure is carried out by tuning the material properties (density, Young's modulus, Poisson's ratio) of each component within their physical property limits as proposed by Ouyang et al.[20]. This procedure is initially conducted on the following components: i) brake disc; ii) backing plate of the brake pad; iii) caliper; and iv) carrier. For each component, the density is determined from measured mass and calculated volume (from the computational models). Furthermore, Young's modulus and Poisson's ratio of these components are determined based on the material type, and the eigenvalue analysis are initialized accordingly. For instance, the brake disc is made of cast iron (GG20), backing plate of the brake pad is steel and the caliper and carrier are gray cast iron (GGG50). As a result of the model updating procedure, the material properties utilized for the brake system components are summarized in Table 2. The modal updating procedure performed on relevant components (as listed in Table 2) has revealed that the Poisson's ratio has minimal effect on the natural frequencies and modes. However, the analysis of brake pad friction material requires an in-depth analysis where the Poisson's ratio may have significant contribution[21]. The friction material of the brake pad is composed of nonferrous metals, organic and inorganic fibers, lubricants, abrasives, property modifiers, etc. Thus, the friction material is modeled as a transversely isotropic material, which has the same physical properties in the transversal plane while assuming different properties in the normal direction. Note that the properties of the friction material are expected to significantly vary due to the composition and production variability. Therefore, properties of the friction material that minimize the deviation from measurements are estimated with a design of experiment study where 125 variants are considered. In this design of experiment study, the following material properties are assumed as independent elastic constants: i) Young's modulus in the transversal plane (E_x and E_y); ii) Young's modulus in the

Table 2—Material properties of the brake system components.

Component	Density (kg/m^3)	Young's modulus (GPa)	Poisson's ratio
Brake disc	7100	110	0.26
Backing plate	7850	210	0.30
Caliper	7100	162	0.30
Carrier	7100	162	0.30

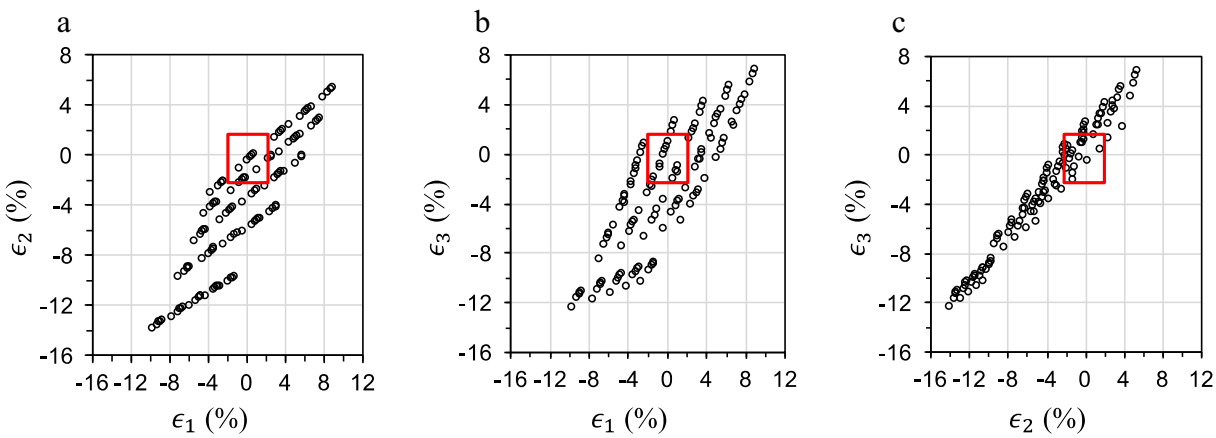

Fig. 5—Comparison between natural frequency errors for each variant of the brake pad material characteristics. (a) Errors in mode 1 vs. mode 2; (b) Errors in mode 1 vs. mode 3; (c) Errors in mode 2 vs. mode 3.

Table 3—Material properties of the brake pad friction material based on the design of experiment analysis.

Parameter set no.	Young's modulus in transversal plane, $E_x = E_y$ (GPa)	Young's modulus in normal direction, E_z (GPa)	Shear modulus in normal direction, $G_{xz} = G_{yz}$ (GPa)	Poisson's ratio in transversal plane, v_{xy}	Poisson's ratio in normal direction, $v_{xz} = v_{yz}$
1	9000	1800	3000	0.20	0.20
2	9000	2000	3000	0.20	0.20
3	9700	1000	3000	0.20	0.20
4	9000	3000	2750	0.20	0.20

normal direction (E_z); iii) shear modulus in the normal direction (G_{xz} and G_{yz}); iv) Poisson's ratio in the transversal plane (v_{xy}); and v) Poisson's ration in the normal direction (v_{xz} and v_{yz}). The first three (predicted) natural frequencies of all variants are compared with measured natural frequencies, and their errors are displayed in Fig. 5. Note that the rectangular regions at the center of the plots denote the variants that lead to minimal error (say less than 2%). It is observed that only four sets of friction material properties fall within the 2% error region as indicated in Table 3, and finally the parameter set 1 is selected for further analysis.

2.3 Validation of Computational Modal Analysis Results

Measured and computed natural frequencies are tabulated in Table 4 along with the prediction errors. Observe that the number of natural modes detected over the frequency range of interest is 11, 3, 4 and 12 for brake disc, brake pad, caliper and carrier, respectively. Observe a good correlation between experimental and computational results as the maximum prediction error is less than 10%. Furthermore, mode shapes that are experimentally (EMA) and computationally (FEM) obtained are displayed in Figs. 6 to 9. Note that the mode shapes from the experimental modal analysis are depicted in wireframe form for the sake of clarity.

Mode shapes of the brake disc are all in-plane modes (Fig. 6) and are well correlated with the mode shapes obtained from the experimental modal analysis. Furthermore, mode shapes of the brake pad are compared in Fig. 7, where two bending (mode 1 and mode 3) and one torsional (mode 2) modes are observed. Again, all three predicted modes match well with measurements. Mode shapes of caliper are compared in Fig. 8, where the significant

Table 4—Validation of computed (f_{FEM}) natural frequencies using experimental modal analysis (f_{EMA}) and corresponding error (ϵ, % $= 100 \times |f_{EMA} - f_{FEM}| / f_{EMA}$) for the brake system components.

Mode index	Brake system components											
	Brake disc			Brake pad			Caliper			Carrier		
	f_{EMA} (Hz)	f_{FEM} (Hz)	ϵ (%)	f_{EMA} (Hz)	f_{FEM} (Hz)	ϵ (%)	f_{EMA} (Hz)	f_{FEM} (Hz)	ϵ (%)	f_{EMA} (Hz)	f_{FEM} (Hz)	ϵ (%)
1	926	935	0.97	3716	3723	0.19	1728	1740	0.69	1006	978	2.78
2	1508	1656	9.81	5572	5558	0.25	2550	2762	8.31	1054	1035	1.80
3	1778	1845	3.77	7738	7837	1.28	3084	3106	0.71	1438	1521	5.77
4	2014	2167	7.60	—	—	—	3502	3460	1.20	1648	1697	2.97
5	2336	2398	2.65	—	—	—	—	—	—	2632	2634	0.08
6	2628	2567	2.32	—	—	—	—	—	—	2904	2896	0.28
7	3684	3699	0.41	—	—	—	—	—	—	3478	3484	0.17
8	4456	4362	2.11	—	—	—	—	—	—	4328	4312	0.37
9	4920	4907	0.26	—	—	—	—	—	—	4996	5015	0.38
10	5590	5613	0.41	—	—	—	—	—	—	5716	5645	1.24
11	6280	6301	0.33	—	—	—	—	—	—	5946	6060	1.92
12	—	—	—	—	—	—	—	—	—	6814	6752	0.91

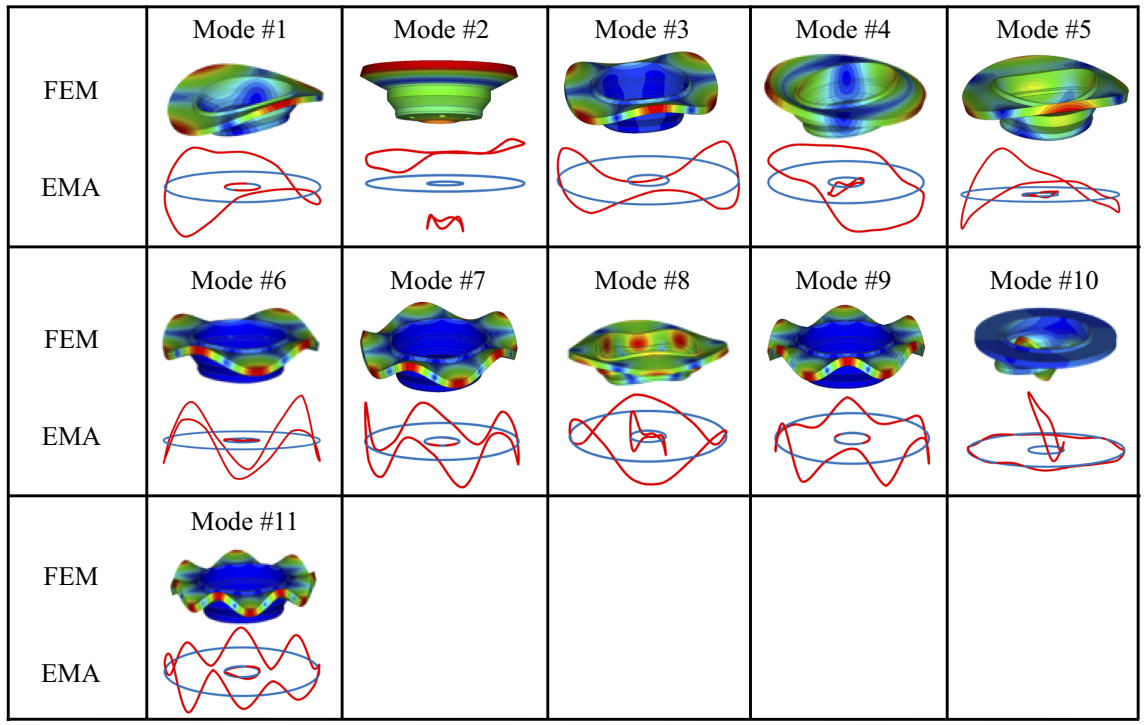

Fig. 6—Experimental and computational mode shapes for the brake disc; refer to Table 2 for natural frequencies. Here, blue and red frames denote the non-deformed and deformed shapes, respectively.

motion is found on the fingers and guide pin housings. As evident from this figure, there is a good match between computational and experimental mode shapes. Finally, the mode shapes of the carrier are shown in Fig. 9. Observe that the mode shapes determined by EMA and FEM match well. In summary, the computational models of the brake system components are experimentally validated based on their natural frequencies and mode shapes.

3 BRAKE SQUEAL STUDIES

3.1 Experimental Investigation of Brake Squeal

In order to investigate the brake squeal phenomenon, a laboratory experiment is designed and built as illustrated schematically in Fig. 10. In this experiment, a brake corner assembly (excluding the suspension system) is driven by

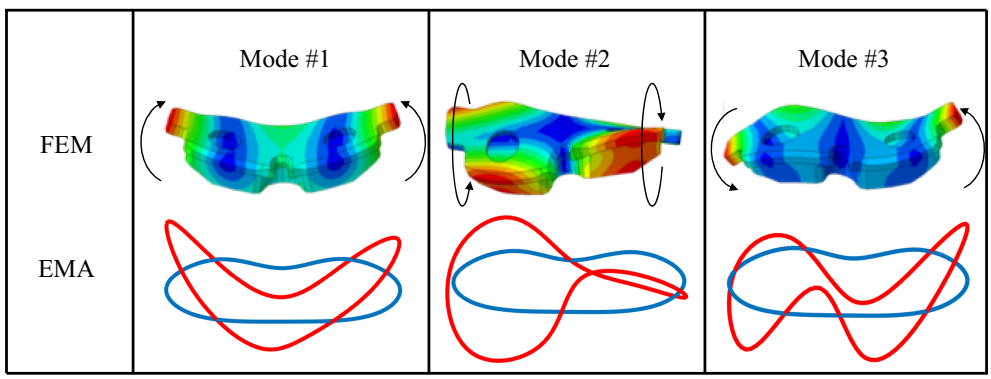

Fig. 7—Experimental and computational mode shapes for the brake pad; refer to Table 2 for natural frequencies. Here, blue and red frames denote the non-deformed and deformed shapes, respectively.

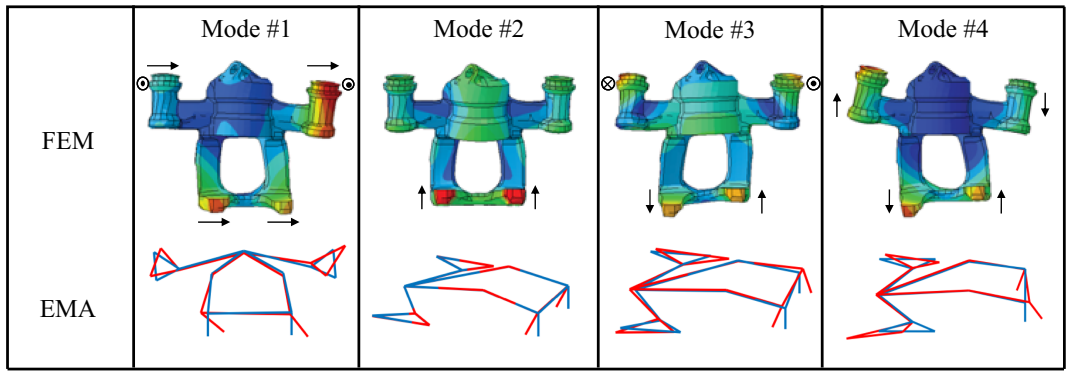

Fig. 8—Experimental and computational mode shapes for the caliper; refer to Table 2 for natural frequencies. Here, blue and red frames denote the non-deformed and deformed shapes, respectively.

an electric motor, and the braking action is generated with a pneumatic actuator. During the experiments, brake disc is first brought to constant speed and then the brakes are applied. The following measurements are acquired during the squeal events: sound pressure with a microphone, acceleration of caliper with a uniaxial accelerometer, hydraulic brake pressure with a pressure transducer, shaft angular speed with an optical tachometer, and brake disc temperature with an infrared thermometer. The experiments are performed in a semi-anechoic room, and the data is acquired with 20 kHz sampling frequency over a time duration of 20 seconds.

In order to determine the most critical operational parameters at which squeal occurs, tests are conducted over a wide range of hydraulic brake pressure and angular speed levels. Additionally, tests are conducted at lower brake disc temperatures (less than 50 °C) in order to minimize any thermal effects; when the brake disc temperature is high, the experiment is paused until the brake disc cools down to a desired temperature. Measurements are recorded only when the squeal noise is detected, and the operational conditions are noted.

Based on the abovementioned experiments, 30 squeal events are detected and their frequencies are mostly around

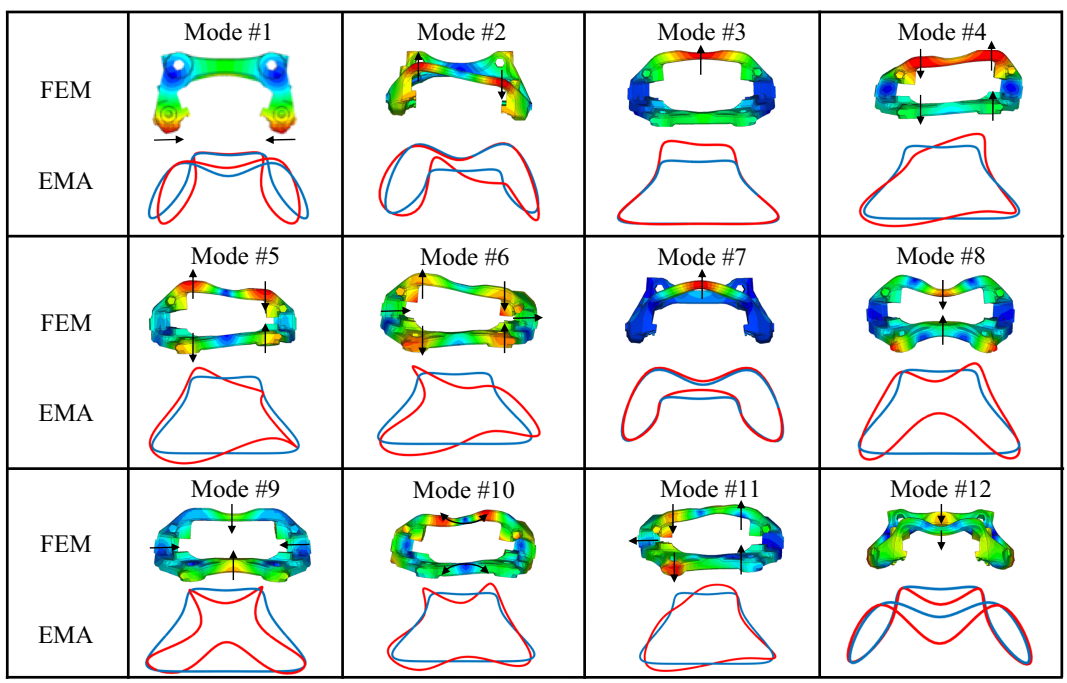

Fig. 9—Experimental and computational mode shapes for the carrier; refer to Table 2 for natural frequencies. Here, blue and red frames denote the non-deformed and deformed shapes, respectively.

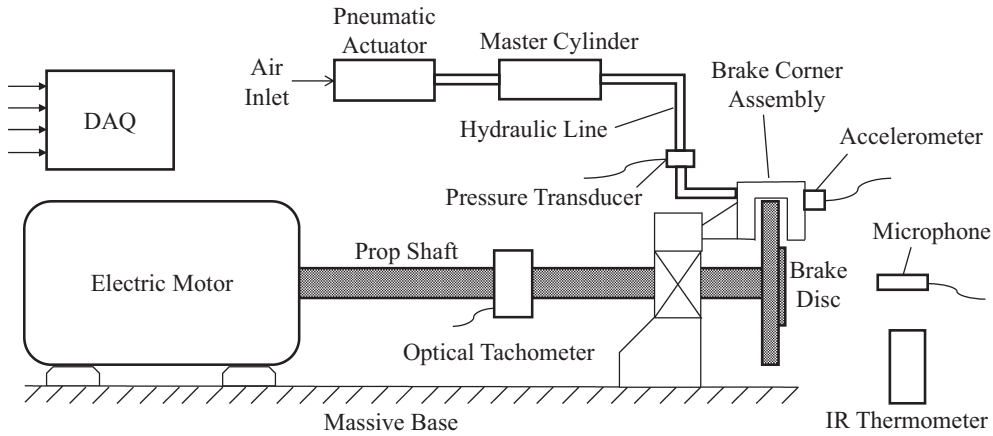

Fig. 10—Schematic of the brake corner experiment and instrumentation used for brake squeal studies.

2400, 3400, 6800 and 9800 Hz as shown in Fig. 11 along with measured (peak) sound pressures. The most significant peak is detected at 3400 Hz, and the peak at 6800 Hz appears to be its super harmonic due to the friction nonlinearities. Furthermore, hydraulic brake pressure and brake disc angular speed ranges where intense squeal noise is observed are determined to be from 3.3 to 4.3 bar and from 40 to 90 rpm, respectively. Distribution of frequencies at which squeal events are observed is displayed in Figs. 12(a) and 12(b) with respect to hydraulic brake pressure and brake disc angular speed, respectively. Observe that a few events are also detected at lower hydraulic brake pressures, but the brake system is more prone to generate squeal noise between 3.8 and 4.3 bar. In terms of the disc angular speed, it is most likely to observe squeal event at lower speeds. Thus, most squeal events are observed over 40 to 60 rpm interval.

Measured time histories of sound pressure and acceleration data at 3.9 bar and 70 rpm are shown in Fig. 13. As evident from the figure, the squeal event is almost periodic though the amplitudes increase successively in both measured sound pressure and acceleration. The narrow band frequency spectra of these data (with a frequency resolution of 0.61 Hz) are depicted in Fig. 14, where a significant peak appears at 2495 Hz. Also, its second harmonic at 4990 Hz is observed in both sound pressure and acceleration spectra. Yet another typical measurement of sound pressure and acceleration time histories at 3.9 bar and 45 rpm are shown in Fig. 15. The squeal is again observed as the successive amplification of almost periodic sound pressure and acceleration responses. Now the fundamental frequency appears at 3420 Hz in this measurement (as shown in Fig. 16) though another peak at 2480 Hz is close to the frequency (2495 Hz) for this case as previously

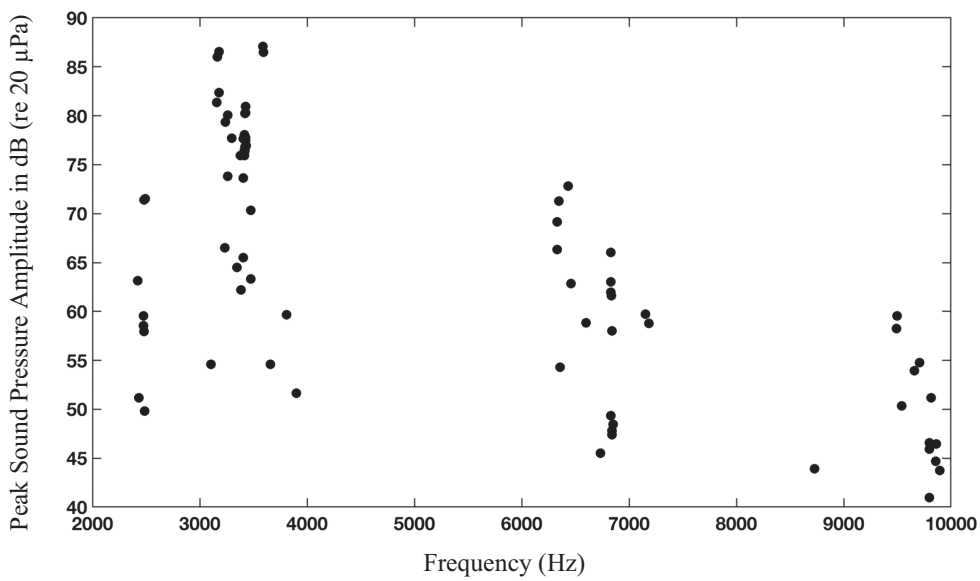

Fig. 11—Measured sound pressure (peak) levels and corresponding squeal frequencies.

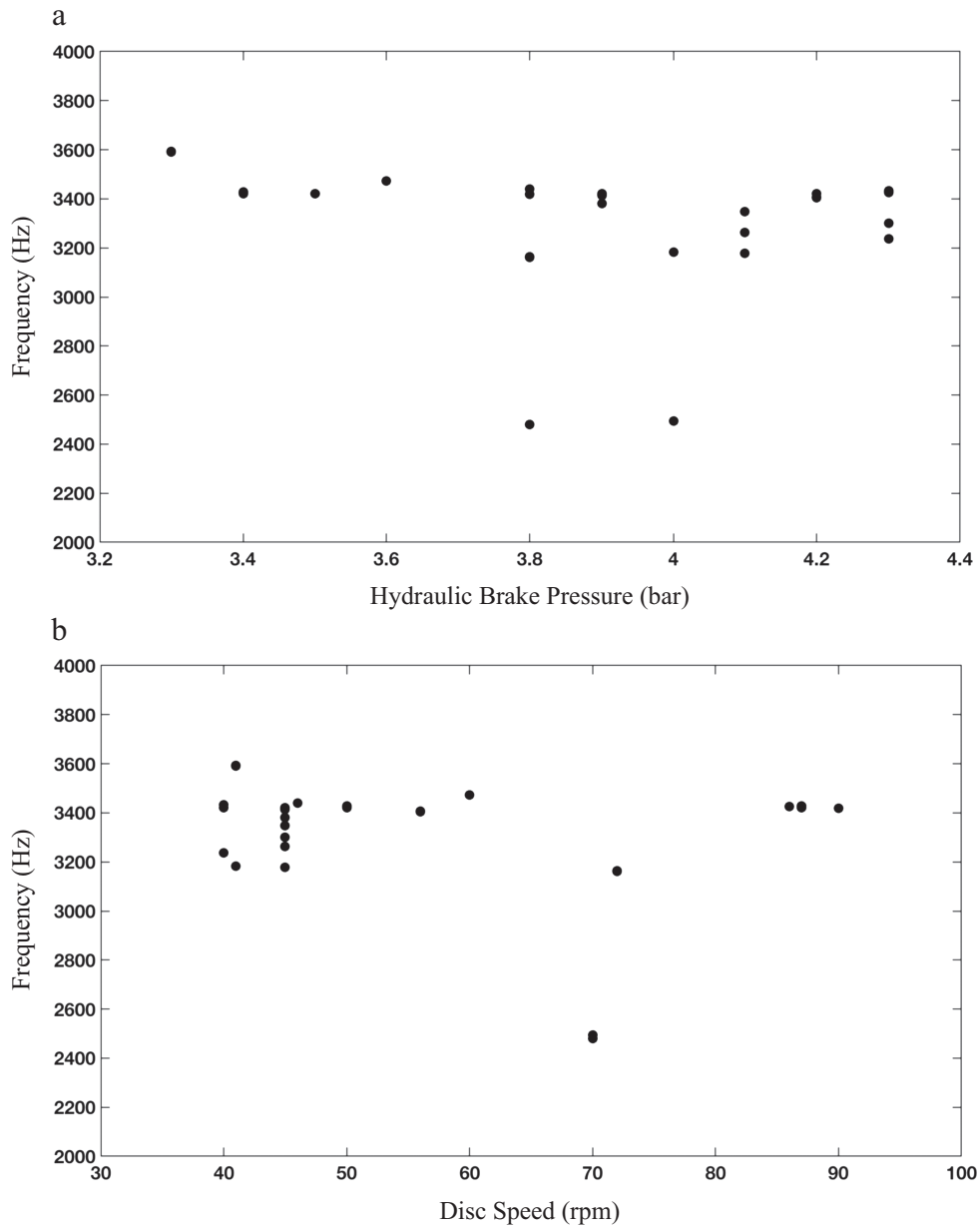

Fig. 12—Variation in squeal frequencies. (a) Effect of the hydraulic brake pressure; (b) Effect of the brake disc speed.

shown in Fig. 14. Similarly, the second harmonic (of the fundamental frequency) again appears at 6840 Hz in both sound pressure and acceleration spectra.

3.2 Computational Model of the Brake Corner Assembly

The computational model of the entire brake system assembly is constructed using the experimentally validated brake system components as discussed in Sec. 2. Of most importance are surface to surface contacts that are defined at the following interfaces: i) brake pad and brake disc; ii) caliper and finger side pad backing plate; and iii) piston and piston side pad backing plate. In order to determine the dynamically unstable (squeal) frequencies, the complex eigenvalue analysis is conducted on the assembly using the following procedure: a) contacts between backing plates and carrier clips are stabilized and brake pressure is applied on the piston and caliper; b) an angular speed is imposed on the brake disc while assuming a constant static friction coefficient at brake disc/brake pad contact interface; a) real eigensolutions are calculated first for the undamped system; and d) complex eigensolutions (including the natural frequencies and mode shapes of the assembly) are finally obtained.

The computational simulations are conducted at those operational conditions where the squeal events are experimentally observed, i.e., over 3.3–4.3 bar and 40–90 rpm.

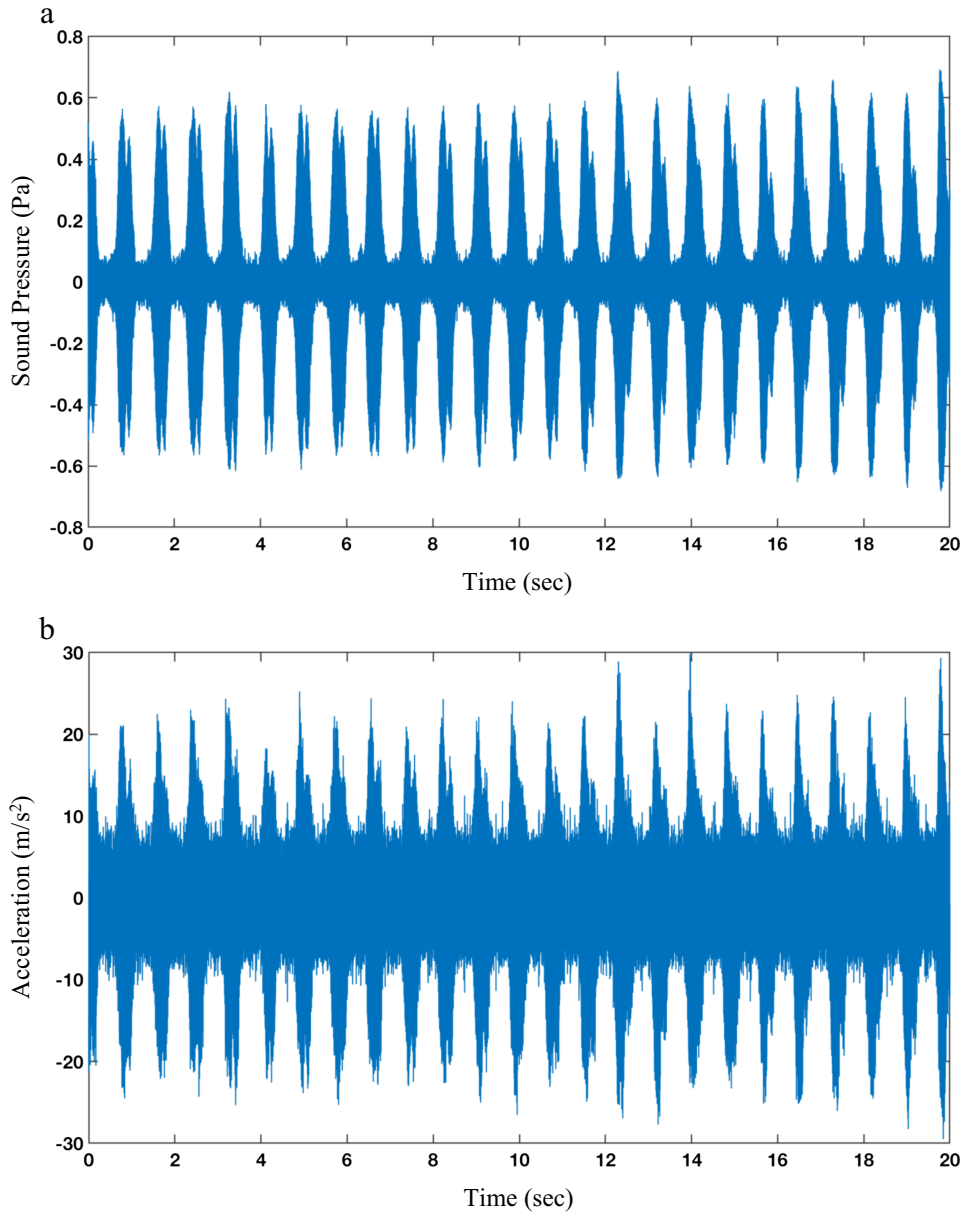

Fig. 13—Measured brake squeal time histories at 3.9 bar and 70 rpm. (a) Sound pressure; (b) Acceleration.

Furthermore, simulations are run at alternate values of friction coefficient at the brake disc/brake pad contact interface and unstable frequencies (that may lead to squeal noise) are determined.

3.3 Validation of Computational Model of Squeal Phenomenon

As mentioned, computational eigenvalue analysis is performed at alternate values of the brake disc/brake pad contact interface friction coefficient, such as 0.3, 0.4, 0.5 and 0.6. Based on these results, two major unstable frequencies are found at 2468 Hz (with a friction coefficient of 0.6) and 3514 Hz (with a friction coefficient of 0.4). Yet other unstable frequencies, say around 4200 Hz, 5800 Hz and 9000 Hz, are also found, but their mode shapes suggest that these frequencies are associated with the motions of brake pad clips. Mode shapes at the dominant frequencies (2468 Hz and 3514 Hz) are shown in Fig. 17. As seen from this figure, the brake corner assembly exhibits a combined motion at 2468 or 3514 Hz where all components are involved. Finally, the frequencies where squeal events are detected in both experimental and computational studies are summarized in Table 5.

Two natural modes of the brake disc at the vicinity of the first squeal frequency (2468 Hz) correspond to the fifth (at 2336 Hz) and sixth (2628 Hz) modes (as listed in Table 4 and Fig. 6); both are in-plane modes with two

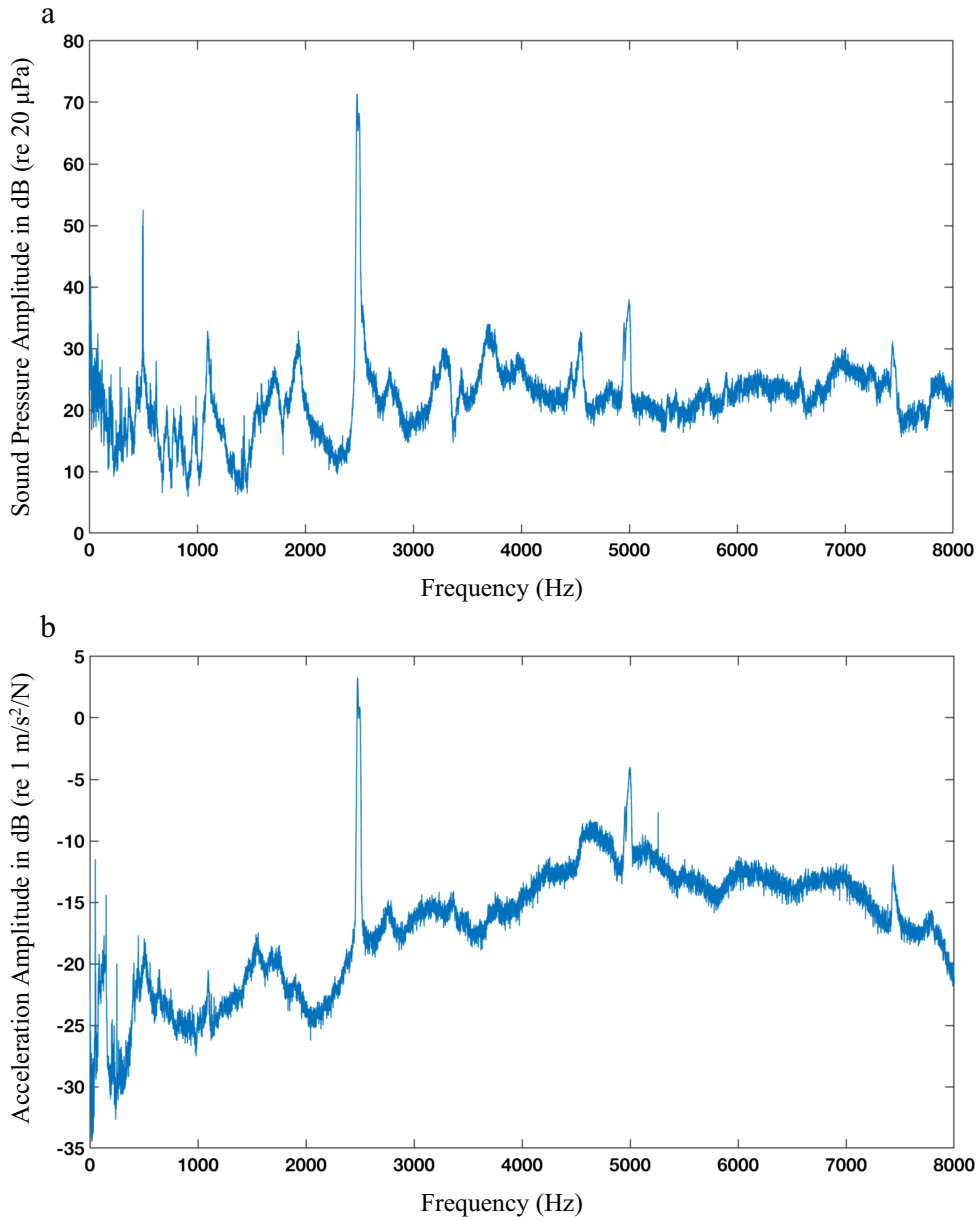

Fig. 14—Narrow band frequency spectra of measured brake squeal signatures at 3.9 bar and 70 rpm. (a) Sound pressure; (b) Acceleration.

and four nodal diameters, respectively. Further, the seventh mode of the brake disc occurs at 3684 Hz (in-plane mode with five nodal diameters) that is close to the second squeal frequency (3514 Hz). Finally, two natural frequencies of caliper (close to the squeal frequencies) at 2550 Hz (second mode) and 3502 Hz (fourth mode) are observed, and their corresponding mode shapes are described as pitch and yaw motions (Table 4 and Fig. 8). Comparing the experimental modal analysis results of brake disc and caliper with the computational model results of Fig. 17 (obtained via the complex eigenvalue analysis at 2468 Hz and 3514 Hz), it is seen that there are two and five nodal diameters, respectively, on the brake disc. Observe that these modes correspond to the fifth and seventh modes of the brake disc that has natural frequencies close to the squeal frequencies. However, the role of caliper motion is not well understood, and thus, the operational deflection shape measurements during the squeal events are performed next.

3.4 Operational Deflection Shape Analysis during Squeal Events

As previously explained, two squeal events are detected during operational experiments that occur at distinct frequencies (2495 Hz and 3420 Hz). For a better understanding of the underlying dynamics that the brake corner assembly exhibits at these frequencies, operational

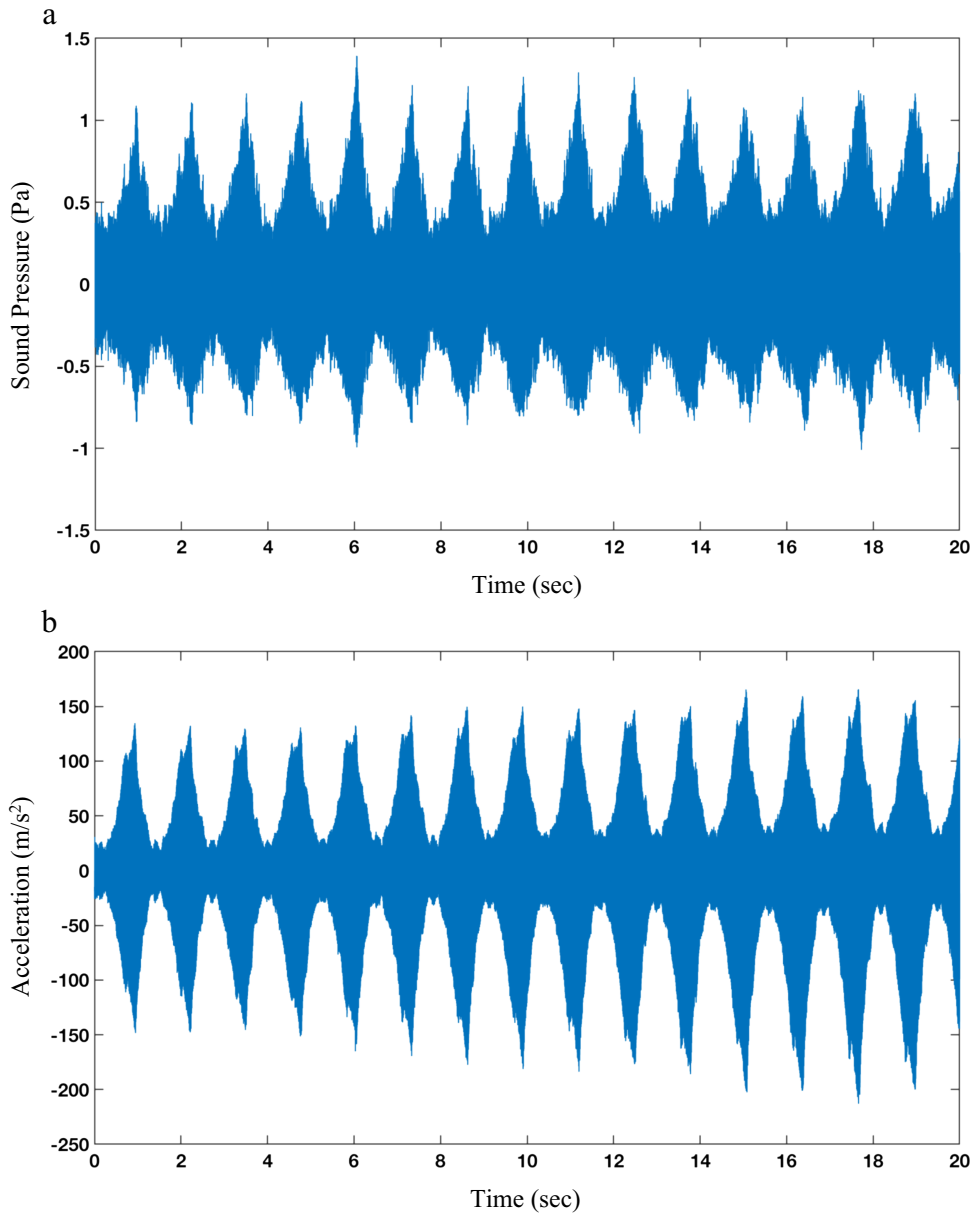

Fig. 15—Measured brake squeal time histories at 3.3 bar and 40 rpm. (a) Sound pressure; (b) Acceleration.

deflection shape (ODS) measurements are conducted on the caliper with eight uniaxial accelerometers. The motion measurement positions are illustrated in Fig. 18, and their role is as follows: i) two accelerometers (denoted 1 and 2) on the tips of the fingers measure in the direction that is orthogonal to the brake disc plane; ii) two accelerometers (3 and 4) at the finger/bridge connections measure in the direction that is orthogonal to brake disc plane; iii) two accelerometers (5 and 6) on the bridges measure in the radial direction of the brake disc; and iv) two accelerometers (7 and 8) on the guide pin housings measure in the radial direction of the brake disc.

The operational deflection shapes determined from 8 measurement locations are depicted in Fig. 19. The motion of the caliper is pitching-like at 2495 Hz, and the caliper motion at 3420 Hz is yaw-like. Hence, the ODS analysis is consistent with mode shapes of the caliper at corresponding frequencies. This leads to the conclusion that the source of the squeal problem (seen in this particular brake corner assembly) is related to the coupling of brake disc and caliper modes under frictional excitation.

4 CONCLUSION

The chief goal of this case study is to examine the brake squeal phenomenon as observed on a particular brake corner assembly (excluding the suspension system) by using well recognized experimental and computational approaches. Accordingly, the objective of this case study

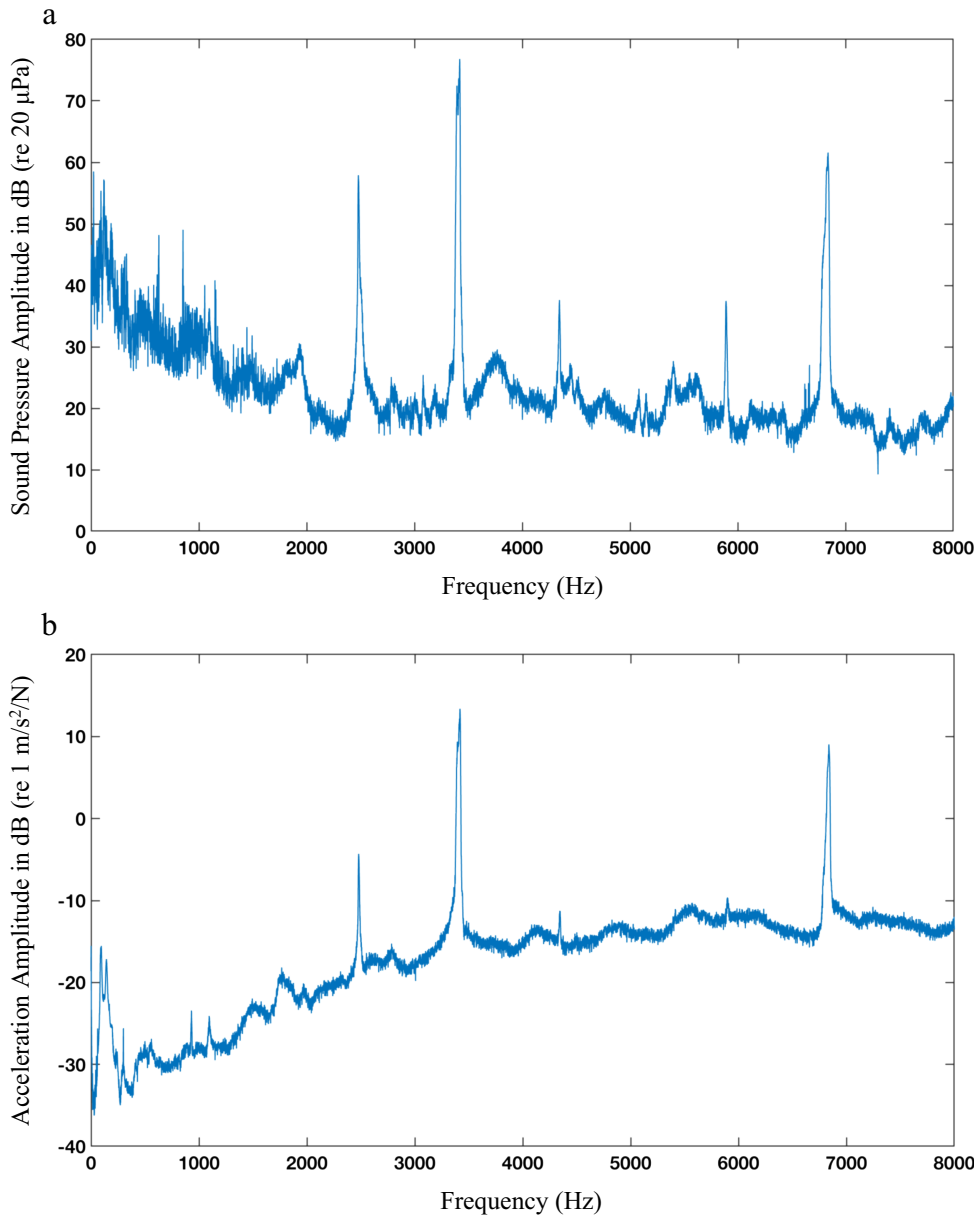

Fig. 16—Narrow band frequency spectra of measured brake squeal signatures at 3.3 bar and 40 rpm. (a) Sound pressure; (b) Acceleration.

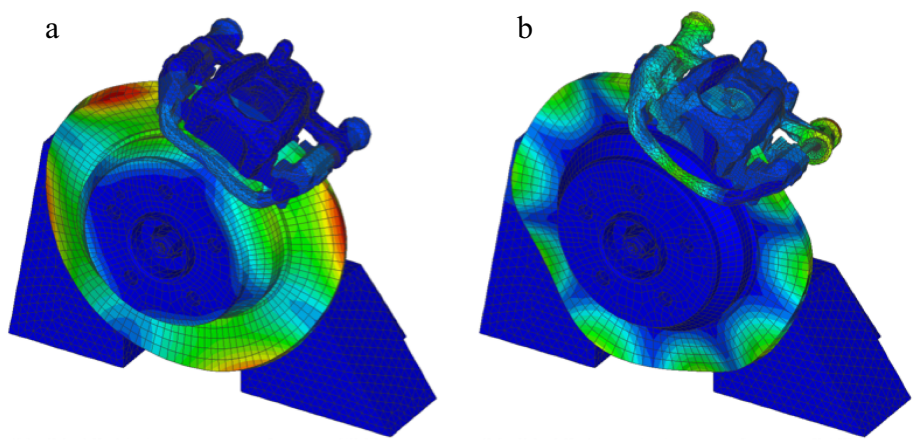

Fig. 17—Mode shapes of the brake corner assembly using FEM. (a) Mode at 2468 Hz; (b) Mode at 3514 Hz.

Table 5—Comparison between experimentally (f_{EXP}) and computationally (f_{FEM}) detected squeal frequencies and corresponding error.

f_{EXP} (Hz)	f_{FEM} (Hz)	$\epsilon = 100 \times \lvert f_{EXP} - f_{FEM} \rvert / f_{EXP}$
2495	2468	1.08%
3420	3514	2.75%

is limited to a thorough investigation of brake squeal problem without proposing any noise control solutions. The modal characteristics of the brake system components are investigated using both experimental (modal tests) and computational (finite element) methods. A good correlation between experimental and computational natural frequencies and mode shapes is obtained, leading to experimentally validated models. Next, a controlled laboratory experiment is designed and built for noise and vibration troubleshooting, and the squeal events are successfully detected at two dominant frequencies. The computational models of the brake system components are also utilized to develop a comprehensive model of the brake corner assembly, and frequencies corresponding to dynamic instability are obtained via the complex eigenvalue analysis method at selected operational conditions. These predicted frequencies are close to the ones experimentally detected. Finally, the operational deflection shape measurements are performed on the laboratory experiment, and motions of the caliper during the squeal events at two frequencies are identified. The complex eigenvalue analysis results exhibit motions similar to those experimentally observed. It is therefore concluded that the squeal problem emerges due to a coupling of the pitch and yaw motions of the caliper where specific modes of the brake disc participate. Finally, this case study clearly illustrates the following guidelines. First, a combined computational and experimental methodology must be employed to gain a better understanding of the squeal noise problem; experimental validation of the brake component or system models is key to a systematic noise control investigation. Second, the squeal noise problem may be reduced or eliminated at the design stage through judicious design modifications via structural finite element models. For instance, certain modes of the brake disc and associated caliper must be well separated in terms of their frequencies. Overall, a better understanding of the squeal noise problem is obtained.

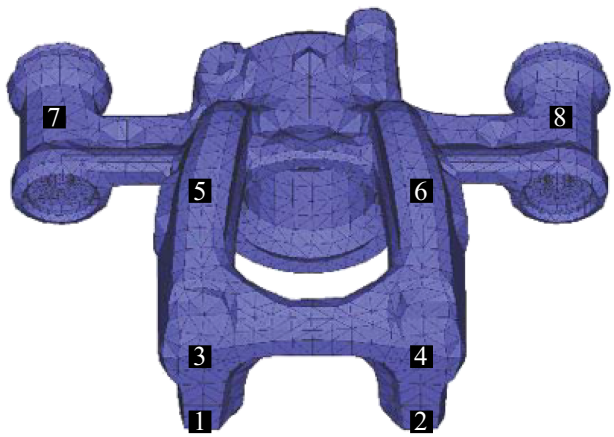

Fig. 18—Accelerometer positions for the operational deflection shape (ODS) measurements.

The scope of this article has been limited to a particular brake corner assembly, and the squeal studies are conducted via a controlled laboratory experiment. It should be mentioned that the dynamic response of the same brake corner assembly in a vehicle may alter due to differing boundary and operational conditions as well as the sensitivities of vehicle transfer paths. In a typical vehicle, the brake corner assembly is coupled to the suspension system which is clearly excluded in the laboratory experiment. Differences due to operational conditions arise

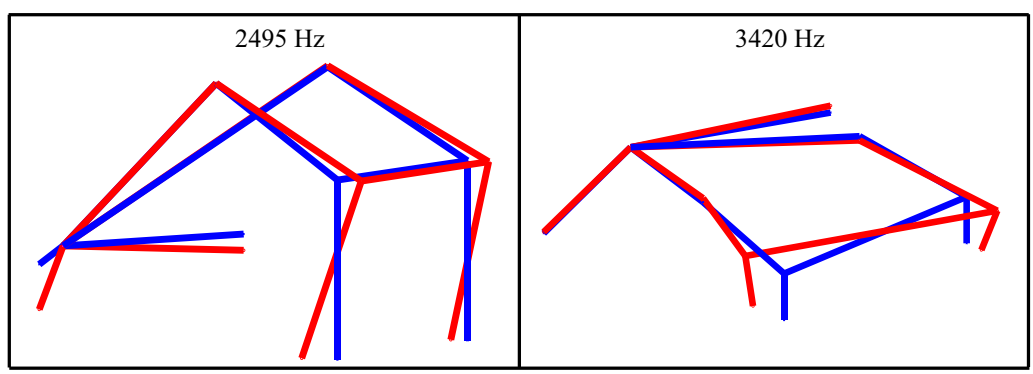

Fig. 19—Operational deflection shapes determined from measurements during the squeal events. Here, blue and red frames denote the non-deformed and deformed shapes, respectively.

mainly due to the hydraulic brake pressure levels applied on the experiment and vehicle. In the experiment, the brake disc is driven by an electric motor, and due to its power limitations, hydraulic brake pressure levels achieved are lower than what are observed on a vehicle. The higher brake pressures in a vehicle lead to higher thermal loads but temperature of the brake corner assembly in the laboratory experiment is kept at lower levels in order to minimize any complications due to the thermal effects. Finally, the computational model is now ready for noise control simulations but vehicle tests must be conducted in order to verify plausible source solutions while resolving the sensitivities of airborne and structureborne paths.

5 ACKNOWLEDGMENTS

The authors acknowledge Mercedes-Benz Turk Inc. for supporting this research. In particular, Hakan Yenerer, Sunay Gunes, and Basaran Ozmen are thanked for their assistance.

6 REFERENCES

1. N.M. Kinkaid, O.M. O'Reilly, and P. Papadopoulos, "Automotive disc brake squeal", *J. Sound Vib.* **267**(1), 105–166, (2003).
2. A. Papinniemi, J.C.S. Lai, J. Zhao, and L. Louder, "Brake squeal: a literature review", *Appl. Acoust.* **63**(4), 391–400, (2002).
3. H. Ouyang, W. Nack, Y. Yuan, and F. Chen, "Numerical analysis of automotive disc brake squeal: a review", *Int. J. Veh. Noise Vib.,* **1**(3/4), 207–231, (2005).
4. M. Yang, A.H. Afaneh and P. Blaschke, "A study of disc brake high frequency squeals and disc in-plane/out-of-plane modes", *SAE Technical Papers* 2003-01-1621, (2003).
5. T. Butlin and J. Woodhouse, "A systematic experimental study of squeal initiation", *J. Sound Vib.,* **330**(21), 5077–5095, (2011).
6. O. Giannini, A. Akay, and F. Massi, "Experimental analysis of brake squeal noise on a laboratory brake setup", *J. Sound Vib.,* **292**(1–2), 1–20, (2006).
7. A. Akay, O. Giannini, F. Massi, and A. Sestieri, "Disc brake squeal characterization through simplified test rigs", *Mech. Syst. Signal Process.,* **23**(8), 2590–2607, (2009).
8. J. Kang, "Finite element modelling for the investigation of in-plane modes and damping shims in disc brake squeal", *J. Sound Vib.,* **331**(9), 2190–2202, (2012).
9. S. Oberst and J.C.S. Lai, "Nonlinear transient and chaotic interactions in disc brake squeal", *J. Sound Vib.*, **342**, 272–289, (2015).
10. F. Massi, L. Baillet, O. Giannini, and A. Sestieri, "Brake squeal: linear and nonlinear numerical approaches", *Mech. Syst. Signal Process.,* **21**(6), 2374–2393, (2007).
11. U.V. Wagner, D. Hochlenert, and P. Hagedorn, "Minimal models for disk brake squeal", *J. Sound Vib.* **302**(3), 527–539, (2007).
12. R.A. Ibrahim, "Friction-induced vibration, chatter, squeal, and chaos. Part II: dynamics and modelling", *Appl. Mech. Rev.,* **47**(7), 227–253, (1994).
13. S. Oberst and J.C.S. Lai, "Chaos in brake squeal", *J. Sound Vib.* **330**(5), 955–975, (2011).
14. T. Tison, A. Heussaff, F. Massa, I. Turpin, and R.F. Nunes, "Improvement in the predictivity of squeal simulations: uncertainty and robustness", *J. Sound Vib.,* **333**(15), 3394–3412, (2014).
15. A.R. AbuBakar and H. Ouyang, "A prediction methodology of disk brake squeal using complex eigenvalue analysis", *Int. J. Veh. Des.* **46**(4), 416–435, (2008).
16. J.J. Sinou, "Transient non-linear dynamic analysis of automotive disc brake squeal — on the need to consider both stability and non-linear analysis", *Mech. Res. Commun.,* **37**(1), 96–105, (2010).
17. J.J.R. Williams, Z. Zhang, S. Oberst, and J.C.S. Lai, "Model updating of brake components' influence on instability predictions", Proceeding of the 22nd International Congress on Sound and Vibration, Florence, Italy, (2015).
18. N.M.M. Maia, J.M.M. Silva, J. He, N.A.J. Lieven, R.M. Lin, G.W. Skingle, W.-M. To, and A.P.V. Urgueira, *Theoretical and Experimental Modal Analysis*, Research Studies Press, Taunton, UK, (1997).
19. ABAQUS User's Manual, Dassault Systèmes, Providence, RI, USA, (2014).
20. H. Ouyang, Q. Cao, J.E. Mottershead, and T. Treyde, "Vibration and squeal of a disc brake: modelling and experimental results", *Proc. Inst. Mech. Eng., Part D,* **217**(1), 867–875, (2013).
21. A. Meziane, S. D'Errico, L. Baillet and B. Laulagnet, "Instabilities generated by friction in a pad-disc system during the braking process", *Tribol. Int.*, **40**, 1127–1136, (2007).